

Gross-Neveu criticality and Dirac quantum spin liquid emerging in $SU(4)$ extended Hubbard model on square lattice

Yuan Da Liao,^{1,2} Xiao Yan Xu,^{3,*} Zi Yang Meng,^{4,†} and Yang Qi^{1,2,5,‡}

¹*State Key Laboratory of Surface Physics, Fudan University, Shanghai 200438, China*

²*Center for Field Theory and Particle Physics, Department of Physics, Fudan University, Shanghai 200433, China*

³*Key Laboratory of Artificial Structures and Quantum Control (Ministry of Education),*

School of Physics and Astronomy, Shanghai Jiao Tong University, Shanghai 200240, China

⁴*Department of Physics and HKU-UCAS Joint Institute of Theoretical and Computational Physics,*

The University of Hong Kong, Pokfulam Road, Hong Kong SAR, China

⁵*Collaborative Innovation Center of Advanced Microstructures, Nanjing 210093, China*

(Dated: May 17, 2022)

At sufficiently low temperatures, interacting electron systems tend to develop orders. Exceptions are quantum critical point (QCP) and quantum spin liquid (QSL), where fluctuations prevent the highly entangled quantum matter to an ordered state down to the lowest temperature. While the ramification of these states may have appeared in high-temperature superconductors, ultra-cold atoms, frustrated magnets and quantum Moiré materials, their unbiased presence remain elusive in microscopic two-dimensional lattice models. Here, we show by means of large-scale quantum Monte Carlo simulations of correlated electrons on the π -flux square lattice subjected to extended Hubbard interaction, that a Gross-Neveu QCP separating massless Dirac fermions and an columnar valence bond solid at finite interaction, and a possible Dirac QSL at the infinite yet tractable interaction limit emerge in a coherent sequence. These unexpected novel quantum states resides in this simple-looking model, unifying ingredients including emergent symmetry, deconfined fractionalization and the dynamic coupling between emergent matter and gauge fields, will have profound implications both in quantum many-body theory and understanding of the aforementioned experimental systems.

Introduction.— The quantum mechanical description of the relativistic electron is attributed to Dirac, who revealed both its intrinsic angular momentum (the spin), with a half-integer quantum number $S = 1/2$ and the existence of its antiparticle, the positron [1]. We now call these particle fermions and they obey the Fermi-Dirac statistics, which implies that two identical particles cannot occupy the same quantum mechanical state. In case of a vanishing rest mass, the energy of Dirac fermions is a linear function of momentum. Such massless Dirac fermions were recently observed in quantum materials like graphene [2], surfaces of topological insulators [3, 4], kagome metals [5, 6] and twisted bilayer graphene [7–30] and many other Moiré systems [31–38]. The interplay between their Dirac relativistic dispersion and the onsite, extended and long-range Coulomb interactions these fermions experienced in the aforementioned materials is believed to be the magic ingredient that gives rise to the plethora of fascinating observed phenomena and has attracted broad attentions from communities encompassing quantum technology and devices and fundamental theories in condensed matter and high-energy physics.

At the theoretical front, model design, field theoretical analysis and large-scale numerical simulations have already provide valuable results on interacting $SU(2)$ Dirac fermions. Studies of Hubbard-like models on the honeycomb or π -flux square lattice suggested the emergence of exotic phases and phase transitions such as possible spin liquids [39–42], valence bond solid (VBS) states [28, 30, 43, 44], quantum spin Hall states and superconductivity [45–49] and Gross-Neveu and deconfined quantum critical points (QCP) [28, 48, 50–60] at or near half-filling per site per degree of freedom.

It is anticipated that, by assigning more degrees of free-

dom to the Dirac fermions and with the extended interaction beyond onsite Hubbard, the system will acquire larger parameter space and exhibit more interesting behavior. Experimentally, the fermionic alkaline cold-atom arrays could realize the $SU(N)$ group with N upto 10 and substantial progress has been made with magnetism and Mott transition realized [61, 62]. Electrons in the twisted bilayer graphene and other quantum Moiré materials are naturally bestowed with more degrees of freedom such as layer, valley and band and subject to extended and even truly long-range Coulomb interactions [7–15, 42, 63–65]. However, the lack of appropriate model design and the unbiased methodologies prohibits the comprehensive understanding of interacting $SU(N)$ Dirac fermions compared with their $SU(2)$ cousins.

This work will address such lack of concrete knowledge in a decisive manner. Here we show, by means of three different yet complementary quantum Monte Carlo (QMC) simulation techniques on correlated $SU(4)$ Dirac fermions on the π -flux square lattice with extended Hubbard interaction: a Gross-Neveu QCP separating massless Dirac fermions and an columnar VBS (cVBS) at finite interaction, and a Dirac quantum spin liquid (QSL) [66, 67] at the infinite interaction limit emerge in a coherent sequence. We find such unexpected sequence of novel quantum states in the simple-looking model, unify the key ingredients including emergent continuous symmetry [28, 30, 57, 59], deconfined fractionalization [67–69] and the dynamic coupling between emergent matter and gauge fields [67, 70, 71] and therefore provide a solid foundation for the future exploration of the novel quantum matter originated from the interplay of the low-energy relativistic dispersion and strong extended and long-range interactions, resonating with the aforementioned quantum materials and the original insight

from Dirac.

Model and method.— We investigate a $SU(4)$ extended Hubbard model at half-filling on the π -flux square lattice with the Hamiltonian

$$H = - \sum_{\langle ij \rangle, \alpha} t_{ij} \left(c_{i\alpha}^\dagger c_{j\alpha} + \text{H.c.} \right) + U \sum_{\square} (n_{\square} - 2)^2, \quad (1)$$

where $\langle ij \rangle$ represent the nearest neighbors, $c_{i\alpha}^\dagger$ and $c_{i\alpha}$ are creation and annihilation operators for fermions on site i with flavor indices $\alpha \in [1, 4]$ with $SU(4)$ symmetry, $n_{\square} \equiv \frac{1}{4} \sum_{i \in \square} n_i$ denotes the extended particle number operator at \square -plaquette, with $n_i = \sum_{\alpha=1}^4 c_{i\alpha}^\dagger c_{i\alpha}$ and $\langle n_{\square} \rangle = 2$ at half-filling, U is the tunable extended repulsive interaction strength.

As shown in Fig. 1 (a), we set the π -flux hopping amplitude $t_{i,i+\vec{e}_x} = t$ and $t_{i,i+\vec{e}_y} = (-1)^{i_x} t$ respectively, where the position of site i is defined as $\mathbf{r}_i = i_x \vec{e}_x + i_y \vec{e}_y$. As discussed in Ref. [59], the positions of Dirac cones and the way of folding of the first Brillouin zone (BZ) will change with different gauge choice of t_{ij} , however, the distance between two Dirac cones does not. Thus we could perform analysis in the original square lattice BZ, as shown in Fig. 1 (b). We set $t = 1$ as the energy unit throughout the article and the π -flux hopping term on square lattice gives rise to the dispersion $\epsilon(\mathbf{k}) = \pm 2t \sqrt{\cos^2 k_x + \cos^2 k_y}$, with the Dirac cones located at momentum $\mathbf{K}_0 = (\pm \frac{\pi}{2}, \pm \frac{\pi}{2})$, which results in the Dirac semimetal state in the weak coupling region. As the interaction strength increases, it is expected that the Dirac cones will be gapped out (the relativistic Dirac fermions will acquire interaction-generated mass) and an insulating phase stemmed from Mott physics will have the upper hand [72, 73]. In our model, for the extended Hubbard interaction term, the onsite, first and second nearest neighbor repulsions are all considered. Similar to the previous studies [27–30, 59], the Mott insulator phase will require a relative larger U to occur, and in the infinite U limit, a QSL phase may emerge [42].

With the help of particle-hole symmetry, our QMC simulation has no sign problem [74, 75]. To obtain the truly unbiased numerical results, we employ three different but complementary QMC algorithms to yield a consistent picture. Most of data are obtained by projector QMC [76], which is suitable to investigate the ground state properties. In addition, a new projection approach of QMC developed by one of us [42] that can perform simulations at the $U = \infty$ is used here to study the nature of the model in Eq. (1) in the strong coupling limit. What's more, we also apply the finite temperature QMC to investigate the thermodynamic and dynamic properties of different phases. The details of these algorithms can be found in previous studies [27–30, 42, 59] and Supplementary Material (SM) [77]. We just mention to set the discrete time slice $\Delta\tau = 0.1$ and projection length $\Theta = L + 10$ for projector QMC method, and $\Delta\tau = 0.05$ for finite temperature QMC method, and we have simulated the square lattice system with $N = L^2$ sites and the linear size $L = 8, 12, 16, 20, 24, 28$.

Phase diagram — The ground state phase diagram of our model obtained from QMC is shown in Fig. 1 (c). In the weak

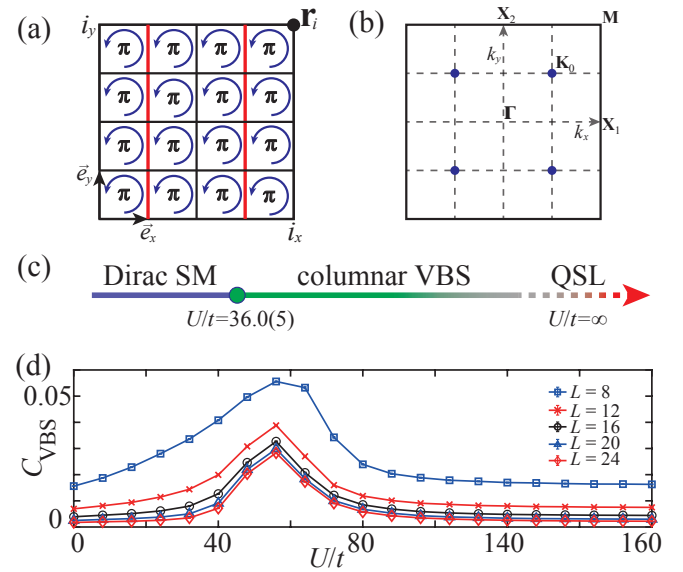


FIG. 1. (a) Square lattice with π -flux hopping. Black and red solid lines denote the hopping amplitude t and $-t$. $\mathbf{r}_i \equiv i_x \vec{e}_x + i_y \vec{e}_y$ is the position of site i , where \vec{e}_x and \vec{e}_y are the unit vector along x and y direction, respectively. (b) The square is the first BZ of the square lattice. The blue solid points represent the positions of Dirac cones at $\mathbf{K}_0 = (\frac{\pi}{2}, \frac{\pi}{2})$. High symmetry points $\Gamma = (0, 0)$, $\mathbf{X}_1 = (\pi, 0)$, $\mathbf{X}_2 = (0, \pi)$ and $\mathbf{M} = (\pi, \pi)$ are denoted. (c) The ground state phase diagram of Eq. (1) obtained from QMC simulations. As explained in the text, there is a gradual change from cVBS to QSL as U approaching the ∞ limit. (d) Structure factor of cVBS as a function of interaction strength for different linear system sizes L .

coupling region, the model features a Dirac semimetal (SM) state due to the stability of relativistic Dirac fermions. Increasing U , the Dirac SM transits into an Mott insulator state with cVBS order via a Gross-Neveu QCP at $U_c/t = 36.0(5)$. Surprisingly, we find as further approaching the strong coupling limit at $U = \infty$, the cVBS gradually evolves into a possible Dirac QSL. From our thermodynamic and dynamic measurements, the Dirac QSL is consistent with the state of emergent spinons with (again) massless Dirac relativistic dispersion coupled with dynamic [possibly U(1)] gauge field. Such a novel state of matter is at the heart of many intriguing quantum many-body phenomena: in condensed matter, the (2 + 1)D field theories with a compact U(1) gauge field coupled to relativistic Dirac fermions often serve as the low-energy effective field theories for high-temperature superconductors [78, 79], algebraic spin liquid [66, 67, 80–85] and the deconfined quantum criticality [68, 86, 87]; in high-energy phase, the mechanism of quark confinement in gauge theories with dynamical fermions such as quantum chromodynamics (QCD) is among the most difficult subjects, and the absence or presence of a deconfined phase in 3D compact quantum electrodynamics (cQED3) coupled to (not necessarily large) flavor massless fermions has attracted a lot of attention and remains unsolved to this day [80, 85, 88–93].

Following our previous study of $SU(2)$ π -flux square lattice

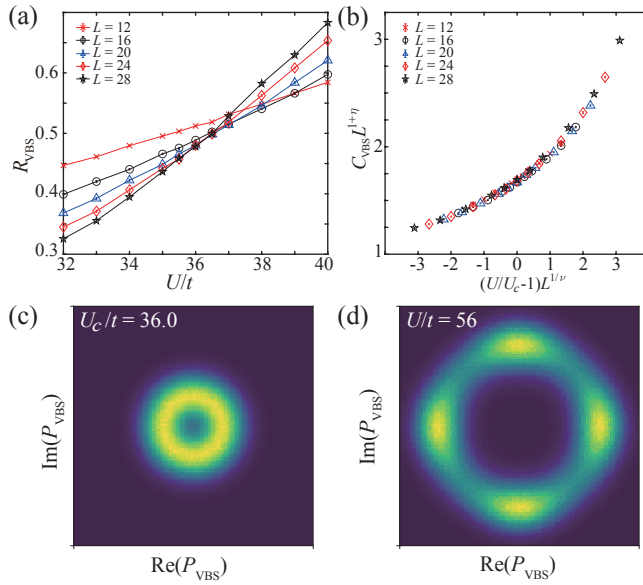


FIG. 2. (a) Correlation ratio of VBS order in Eq. (4), the crossing point is the Dirac SM to cVBS Gross-Neveu QCP. (b) Data collapse of VBS structure factor. The data cross and collapse give an estimate of the position of QCP at $U_c/t = 36.0(5)$ with the critical exponents $\nu = 1.00(5)$ and $\eta = 0.86(4)$. (c) The histogram of P_{VBS} at U_c . There is an emergent $U(1)$ symmetry associated with the Gross-Neveu transition. (d) The histogram of P_{VBS} at $U > U_c$. The angular distribution is consistent with cVBS order.

extended Hubbard model [59], to confirm the VBS order, we define the VBS structure factor

$$C_{\text{VBS}}^{\mathbf{e}}(\mathbf{k}, L) = \frac{1}{L^4} \sum_{i,j} e^{i\mathbf{k} \cdot (\mathbf{r}_i - \mathbf{r}_j)} \langle B_i^{\mathbf{e}} B_j^{\mathbf{e}} \rangle, \quad (2)$$

where $B_i^{\mathbf{e}} = \frac{1}{4} \sum_{\alpha=1}^4 \left(t_{i,i+\mathbf{e}} c_{i,\alpha}^\dagger c_{i+\mathbf{e},\alpha} + \text{H.c.} \right)$ are gauge invariant bond operators with \mathbf{e} standing for \vec{e}_x or \vec{e}_y . For cVBS order, $C_{\text{VBS}}^{\vec{e}_x}(\mathbf{k}, L)$ is peaked at momentum $\mathbf{X}_1 = (\pi, 0)$ and $C_{\text{VBS}}^{\vec{e}_y}(\mathbf{k}, L)$ is peaked at momentum $\mathbf{X}_2 = (0, \pi)$. Since the perfect cVBS order has Z_4 degeneracy on square lattice, $C_{\text{VBS}}^{\vec{e}_x}(\mathbf{X}_1, L)$ should be equivalent to $C_{\text{VBS}}^{\vec{e}_y}(\mathbf{X}_2, L)$ in ideal QMC simulations. Consequently, we can define the square of the cVBS order parameter as

$$C_{\text{VBS}}(L) = C_{\text{VBS}}^{\vec{e}_x}(\mathbf{X}_1, L) + C_{\text{VBS}}^{\vec{e}_y}(\mathbf{X}_2, L). \quad (3)$$

As shown in Fig. 1 (d), as tuning U/t from 0 to 160, C_{VBS} first increases then decreases, which means our model transits from Dirac SM to cVBS order, then cVBS order becomes weaker and gradually evolves into a possible Dirac QSL phase at the $U = \infty$ limit. We also calculate the square of antiferromagnetic (AF) order parameter and extrapolate it to the thermodynamic limit (shown in SM [77]) and do not find AF order in all parameter region simulated. These results are summarized as the phase diagram in Fig. 1 (c), and we now discuss in detail the sequence of phases and phase transitions along the U/t parameter path.

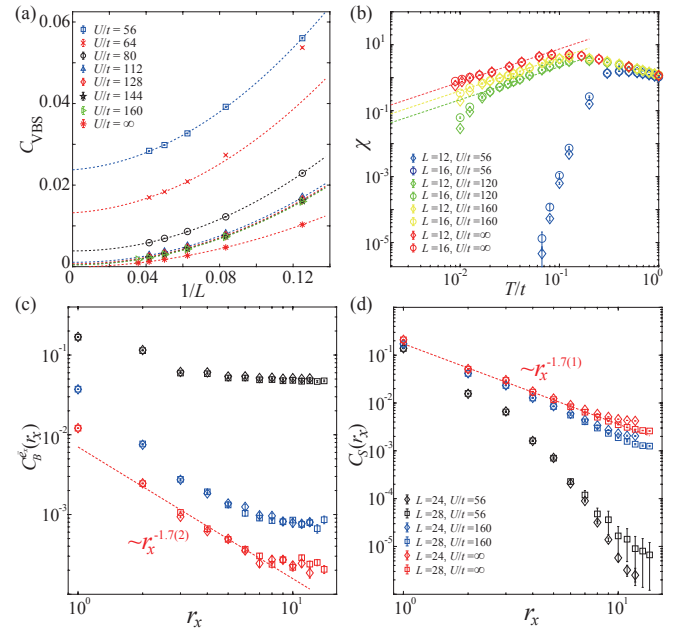


FIG. 3. (a) $1/L$ extrapolation of C_{VBS} . The dash lines are quadratic polynomial fittings through the data points. As $U \rightarrow \infty$ the cVBS order extracts to vanishing small values. (b) Log-log plot of spin susceptibility χ as function of T for different L and U . The dash lines, drawn as guide to the eyes, represent the linear functions $\chi = aT$ for different constant a . (c) Log-log plots of $C_B^{\vec{e}_x}(r_x)$ and (d) $C_S(r_x)$ as function of r_x for different L and U . They have the same power-law decay as $1/r_x^{1.7}$ at $U = \infty$. The linear fitting with least squares method are used.

Gross-Neveu transition and the Dirac QSL— We first focus on the Gross-Neveu QCP between the Dirac SM and cVBS state. To locate the corresponding QCP, we define the correlation ratio of cVBS order as

$$R_{\text{VBS}}(L) = 1 - \frac{C_{\text{VBS}}^{\vec{e}_x}(\mathbf{X}_1 + d\mathbf{q}, L)}{2C_{\text{VBS}}^{\vec{e}_x}(\mathbf{X}_1, L)} - \frac{C_{\text{VBS}}^{\vec{e}_y}(\mathbf{X}_2 + d\mathbf{q}, L)}{2C_{\text{VBS}}^{\vec{e}_y}(\mathbf{X}_2, L)}, \quad (4)$$

where $d\mathbf{q}$ is the smallest momentum in finite-size BZ. $R_{\text{VBS}}(L)$ will approach to 1 (0) in an ordered (disordered) phase. This dimensionless quantity is scale invariant at the QCP for sufficiently large system size [43, 44, 52, 59, 94], which renders a crossing point $U_c/t = 36.0(5)$ as the position of the QCP among different L , shown in Fig. 2 (a). Near the QCP, the cVBS structure factor should obey the scaling relation $C_{\text{VBS}}(L) = L^{-z-\eta} f(L^{1/\nu}(U - U_c)/U_c)$, where f is the scaling function, z is the dynamical exponent and should be set as 1 for relativistic Dirac fermions. With this scaling relation, we collapse $C_{\text{VBS}}(L)$, as shown in Fig. 2(b), and extract the universal critical exponents $\nu = 1.00(5)$ and $\eta = 0.86(4)$. In principle, there are two kinds of VBS order, cVBS and plaquette VBS (pVBS), that share the same order parameter. To further verify the cVBS order is in our model, we define the

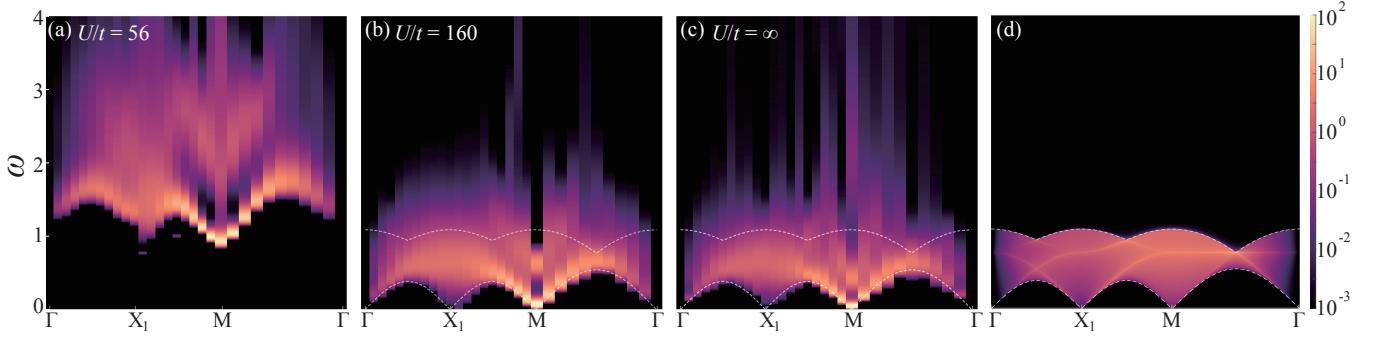


FIG. 4. Dynamic spin spectra obtained from QMC-SAC calculations as a sequence inside the cVBS phase, towards and inside the Dirac QSL with $L = 20$. (a) is inside the cVBS phase with $U/t = 56$, (b) is close to the $U = \infty$ limit with $U/t = 160$ and (c) is exactly at the $U = \infty$ limit. (d) The dynamical spin spectrum of free π -flux Dirac fermions. The lower and upper dashed curves in (b), (c) and (d) trace out the lower and upper edges of the two-spinon continuum, i.e. $\omega^{\text{lower}}(\mathbf{q}) \propto \min_{\mathbf{k} \in \text{BZ}} |\epsilon(\mathbf{k}) + \epsilon(\mathbf{q} - \mathbf{k})|$ and $\omega^{\text{upper}}(\mathbf{q}) \propto \max_{\mathbf{k} \in \text{BZ}} |\epsilon(\mathbf{k}) + \epsilon(\mathbf{q} - \mathbf{k})|$, assuming free spinons with the π -flux state dispersion. The calculation of the free two-spinon continuum is shown in SM [77].

order parameter histogram

$$\begin{aligned} P_1 &= \left(1/L^2\right) \sum_i \left(B_i^{\vec{e}_y} + \omega B_i^{-\vec{e}_x} + \omega^2 B_i^{-\vec{e}_y} + \omega^3 B_i^{\vec{e}_x} \right) e^{i\mathbf{X}_1 \cdot \mathbf{r}_i}, \\ P_2 &= \left(1/L^2\right) \sum_i \left(B_i^{\vec{e}_y} + \omega B_i^{-\vec{e}_x} + \omega^2 B_i^{-\vec{e}_y} + \omega^3 B_i^{\vec{e}_x} \right) e^{i\mathbf{X}_2 \cdot \mathbf{r}_i}, \\ P_{\text{VBS}} &= P_1 + P_2 \end{aligned} \quad (5)$$

with $\omega = i$. For cVBS, the angular distribution of the complex number P_{VBS} will peak at the angles $(0, \frac{\pi}{2}, \pi, \frac{3\pi}{2})$, while for pVBS, it will peak at $(\frac{\pi}{4}, \frac{3\pi}{4}, \frac{5\pi}{4}, \frac{7\pi}{4})$. Our numerical result, as shown in Fig. 2(d), confirm the cVBS. More interestingly, as shown in Fig. 2(c), there is an emergent $U(1)$ symmetry at U_c , which suggests that the corresponding QCP should be described by the 3D $N = 4$ chiral Gross-Neveu XY universality class [57, 71, 95–98]. Our extracted critical exponent ν and η are comparable with the previous QMC [28, 96, 99] and $4 - \epsilon$ expansion [100, 101] results on the same universality class.

Next, we move on to the stronger interaction regime. As shown in Fig. 3 (a), we extrapolate the cVBS structure factors to the thermodynamic limit for different $U > U_c$. We notice that the VBS order becomes weaker as increasing U and almost vanishes with the system sizes accessed for finite U QMC around $U/t = 160$. Our $U = \infty$ QMC simulations consistently reveal the C_{VBS} extrapolate to 0 at the strong interaction limit (the absence of the AF order on entire phase diagram is shown in the SM [77]), which indicate an emergent QSL state. According to the theory of algebraic QSL with Dirac spinons coupled to $U(1)$ gauge field [80, 82], besides the absence of AF and VBS order parameters, the bond operator correlation

$$C_B^{\vec{e}_x}(\mathbf{r}) \equiv e^{-i\mathbf{X}_1 \cdot \mathbf{r}} \left(\langle B_i^{\vec{e}_x} B_j^{\vec{e}_x} \rangle - \langle B_i^{\vec{e}_x} \rangle \langle B_j^{\vec{e}_x} \rangle \right) \quad (6)$$

and the AF (staggered) spin correlation

$$C_S(\mathbf{r}) \equiv e^{-i\mathbf{M} \cdot \mathbf{r}} \sum_{\alpha, \beta} \langle S_\beta^\alpha(i) S_\alpha^\beta(j) \rangle \quad (7)$$

should decay algebraically at large separations. In above equations, $\mathbf{r} = \mathbf{r}_i - \mathbf{r}_j$ is the relative distance, $S_\beta^\alpha(i) =$

$c_{i,\alpha}^\dagger c_{i,\beta} - \frac{\delta_{\alpha,\beta}}{4} \sum_\gamma c_{i,\gamma}^\dagger c_{i,\gamma}$ are the $SU(4)$ spin full operators with $\alpha, \beta, \gamma \in [1, 4]$. For both finite and ∞ interaction strength, $C_B^{\vec{e}_x}(\mathbf{r})$ and $C_S(\mathbf{r})$ with largest system sizes are shown in Fig. 3 (c) and (d), and we indeed numerically observe the algebraical behaviors in the correlation functions as $U \rightarrow \infty$. These are strong evidence of the robust existence of QSL. Most interestingly, we find the two correlation functions acquire the same power-law decay within errorbar, i.e. $\sim 1/r^{1.7(2)}$. This is a strong indication that, the QSL phase shall be understood with a low-lying effective theory with emergent relativistic Dirac spinons coupled with dynamic $U(1)$ gauge field, as only in this way, the kinetic bond and $SU(4)$ spin correlation functions, although have different scaling dimension at the bare operator level, actually describe the correlation of the same effective degrees of freedom in low-energy effective field theory multiplet [68, 69, 80, 82, 102, 103]. Furthermore, the decay power indicates it is unlikely to be a \mathbb{Z}_2 -Dirac QSL [104, 105], because the \mathbb{Z}_2 gauge field does not have gapless excitations, and thus does not modify the decay power of free Dirac fermions, which would be 4. However, the decay power is much smaller than previous DQMC and large- N studies [67, 80, 82] of $U(1)$ Dirac QSL (which are both larger than 3). Possible explanations of this discrepancy include finite-size effects, a new QSL state being realized, or that the $U \rightarrow \infty$ limit is a critical point between the VBS phase and a QSL phase instead of the QSL phase itself. We leave this to future works. Last, we notice that a recent work [85] shows the monopole operator may be relevant in $U(1)$ Dirac-QSLs and may lead to instabilities. This may be related to the fact that we only observe QSL in the $U \rightarrow \infty$ limit: it is possible that an effective local constraint enforced by the infinite interaction helps stabilize the QSL phase. We leave detail studies on this issue to future works.

Physical observables for the Dirac QSL— The confirmation of emergent Dirac spinon coupled with $U(1)$ gauge field with power-law correlation functions for bond and spin operators, are still too abstract from the experimental point of view. To this end, we follow the tradition in condensed matter

experiments to further probe the response of the system by external parameters. Here we focus on the thermodynamic and dynamic measurements at the Dirac QSL phase. It was proposed that from the temperature dependence of the magnetic susceptibility, one could expect a $\chi_0 \sim T$ behavior of such U(1) Dirac spin liquid state at low temperatures [66, 81], distinctively different from the $\chi_0 \sim T^{-1}$ for a Pauli paramagnet with Fermi surface. We define dynamic spin correlation function as $\chi_S(\mathbf{q}, \tau) \equiv \frac{1}{L^2} \sum_{\mathbf{r}} e^{-i\mathbf{q} \cdot \mathbf{r}} \sum_{\alpha, \beta} \langle S_{\beta}^{\alpha}(i, \tau) S_{\alpha}^{\beta}(j, 0) \rangle$ with $\tau \in [0, \beta]$, then the susceptibility can be computed as $\chi_0(T) = \int_0^{\beta=1} \chi_S(\mathbf{q} = 0, \tau) d\tau$. As shown in Fig. 3 (b), $\chi_0(T)$, obtained from finite temperature QMC, obviously violate $\chi_0 \sim T$ behavior at $U/t = 56$, where the cVBS order is very strong and the state is gapped at low temperature. However, as increasing interaction weaken the cVBS order, at $U/t = 120$ and $U/t = 160$, $\chi_0 \sim T$ behavior gradually emerge. And at $U = \infty$, i.e. in the Dirac QSL, $\chi_0(T)$ decays as function of temperature is in good agreement with linear behavior.

Moreover, with the good quality dynamic spin correlation function data $\chi_S(\mathbf{q}, \tau)$ at hand, the stochastic analytic continuation (SAC) scheme [77] can reveal reliable spectral information, $S(\mathbf{q}, \omega)$, as have been widely tested in fermionic and bosonic quantum many-body systems in 1D, 2D and 3D [64, 71, 106–119], and compared with both neutron scattering and NMR experiments [120, 121] and the exact solution and exact diagonalization numerics [64, 65, 109, 115]. We therefore compute the spin spectrum $S(\mathbf{q}, \omega)$ with QMC+SAC at different U , the spectra are shown in Fig. 4.

By comparison with spin spectra at $U/t = 56$ [Fig. 4 (a)], $U/t = 160$ [Fig. 4 (b)], $U = \infty$ [Fig. 4 (c)] and analytical calculation of free π -flux model on square lattice [Fig. 4 (d)], several exotic features of the spectra can be unambiguously identified. First, we observe broad and prominent continua in $S(\mathbf{q}, \omega)$ at the $U/t = 160$ and $U = \infty$, which reflect the expected fractionalization and emergence of deconfined spinons. In contrast, inside the cVBS phase, the $S(\mathbf{q}, \omega)$ is gapped due to the translational symmetry breaking.

Second, we find that the lower edges of both $U/t = 160$ and $U = \infty$ spectra can be well accounted for by a remarkably simple dispersion relation, $\omega^{\text{lower}}(\mathbf{q}) \propto \min_{\mathbf{k} \in \text{BZ}} |\epsilon(\mathbf{k}) + \epsilon(\mathbf{q} - \mathbf{k})|$ [the lower dashed lines in Fig. 4 (b) and (c)], which matches the dispersion relation of free fermionic spinon in the square lattice π -flux state [the lower dashed lines in Fig. 4 (d)] [68, 71]. This points us to the cQED₃ description of the Dirac QSL state above [67], which is also proposed as the low-energy description of the deconfined quantum critical point [86, 122]. If indeed the broad spectral functions seen in Fig. 4 (b) and (c) are due to two independently propagated spinons, the upper spectral bound can also be obtained by $\omega^{\text{upper}}(\mathbf{q}) \propto \max_{\mathbf{k} \in \text{BZ}} |\epsilon(\mathbf{k}) + \epsilon(\mathbf{q} - \mathbf{k})|$ [the upper dashed lines in Fig. 4 (b), (c) and (d)]. This is only in reasonable agreement with the observed distribution of the main spectral weight, though clearly some weights arising from spinon interactions are also present at higher energies.

Furthermore, gapless continua observed at both \mathbf{X}_1 and \mathbf{M}

points are consistent with the fact in Fig. 3 (c) and (d) both AF (staggered) spin and columnar VBS correlations exhibiting the same power-law decay. The same observation of gapless spin continua at (π, π) and $(\pi, 0)$ have also been confirmed in the $SU(2)$ J-Q model at its deconfined quantum critical point [68]. It was also argued recently that these spectral continua in magnetic models and materials, are evidence for deconfined quantum critical point, in metal-organic compound $\text{Cu}(\text{DCOO})_2 \cdot 4\text{D}_2\text{O}$ and in the Shastry-Sutherland compound $\text{SrCu}_2(\text{BO}_3)_2$ [109, 123–126]. Such spectral signatures can certainly be probed in neutron scattering, RIXS, NMR and scanning tunnelling spectroscopy techniques.

Discussion — As mentioned throughout the paper, the coupling between fermionic matter and gauge fields is of fundamental importance in both high-energy and condensed-matter physics. In the latter, gauge fields can emerge as a consequence of fractionalization in quantum materials, which may be realizable in certain frustrated magnets, such as the recent triangular antiferromagnets NaYbO_2 [127] and $\text{Sr}_3\text{CuSb}_2\text{O}_9$ [128], and kagome antiferromagnet $\text{YC}_{\text{u}}_3(\text{OH})_6\text{Br}_2[\text{Br}_x(\text{OH})_{1-x}]$ [129]. At the model level, prominent proposals have been applied to high-temperatur superconductors [78, 81, 83], QSL [66, 79, 130, 131] and deconfined quantum critical points [68, 69, 86, 87, 102, 132]. But since these strongly correlated quantum states are characterized by topological order or coupled matter fields and gauge fields, it is often-times difficult to unambiguously identify them in simulation with the relevant low-energy fractionalized excitations and their characteristic properties.

In this work, we have overcome these difficulty with model design and numerical methodology development. By means of three different and complementary QMC simulation techniques, we reveal the phase diagram of correlated $SU(4)$ Dirac fermions on the π -flux square lattice with extended Hubbard interaction. We find a Gross-Neveu QCP with emergent U(1) symmetry separating the massless Dirac fermions and an columnar VBS at finite interaction, and a possible Dirac QSL at the infinite interaction limit with its characteristic thermodynamic and dynamic properties accessible to experiments. Such unexpected sequence of novel quantum states in the simple-looking model, unify the key ingredients including emergent symmetry [28, 30, 57, 59], deconfined fractionalization [67–69] and the dynamic coupling between emergent matter and gauge fields [67, 70, 71]. Our work therefore provides a solid foundation for the future exploration of the novel quantum matter originated from the interplay of the low-energy relativistic dispersion and strong extended and long-range interactions.

Acknowledgements — We acknowledge Chong Wang for valuable discussions on the subject. Y.D.L. acknowledges the support of Project funded by China Postdoctoral Science Foundation through Grants No. 2021M700857 and No. 2021TQ0076. X.Y.X. is sponsored by the National Key R&D Program of China (Grant No. 2021YFA1401400), Shanghai Pujiang Program under Grant No. 21PJ1407200, Yangyang Development Fund, and startup funds from SJTU. Z.Y.M. acknowledges support from the Research Grants Council of

Hong Kong SAR of China (Grant Nos. 17303019, 17301420, 17301721 and AoE/P-701/20), the K. C. Wong Education Foundation (Grant No. GJTD-2020-01) and the Seed Funding “Quantum-Inspired explainable-AI” at the HKU-TCL Joint Research Centre for Artificial Intelligence. Y.Q. acknowledges support from the the National Natural Science Foundation of China (Grant Nos. 11874115 and 12174068).

* xiaoyanxu@sjtu.edu.cn

† zymeng@hku.edu.cn

‡ qiyang@fudan.edu.cn

- [1] S. Weinberg, *The quantum theory of fields*, Vol. 2 (Cambridge university press, 1995).
- [2] K. S. Novoselov, A. K. Geim, S. V. Morozov, D. Jiang, M. I. Katsnelson, I. Grigorieva, S. Dubonos, and a. Firsov, *nature* **438**, 197 (2005).
- [3] Y. Chen, J. G. Analytis, J.-H. Chu, Z. Liu, S.-K. Mo, X.-L. Qi, H. Zhang, D. Lu, X. Dai, Z. Fang, *et al.*, *science* **325**, 178 (2009).
- [4] H. Zhang, C.-X. Liu, X.-L. Qi, X. Dai, Z. Fang, and S.-C. Zhang, *Nature physics* **5**, 438 (2009).
- [5] L. Ye, M. Kang, J. Liu, F. von Cube, C. R. Wicker, T. Suzuki, C. Jozwiak, A. Bostwick, E. Rotenberg, D. C. Bell, L. Fu, R. Comin, and J. G. Checkelsky, *Nature* **555**, 638 (2018).
- [6] M. Kang, L. Ye, S. Fang, J.-S. You, A. Levitan, M. Han, J. I. Fazio, C. Jozwiak, A. Bostwick, E. Rotenberg, M. K. Chan, R. D. McDonald, D. Graf, K. Kaznatcheev, E. Vescovo, D. C. Bell, E. Kaxiras, J. van den Brink, M. Richter, M. Prasad Ghimire, J. G. Checkelsky, and R. Comin, *Nature Materials* **19**, 163 (2020).
- [7] R. Bistritzer and A. H. MacDonald, *Proceedings of the National Academy of Sciences* **108**, 12233 (2011).
- [8] Y. Cao, V. Fatemi, A. Demir, S. Fang, S. L. Tomarken, J. Y. Luo, J. D. Sanchez-Yamagishi, K. Watanabe, T. Taniguchi, E. Kaxiras, *et al.*, *Nature* **556**, 80 (2018).
- [9] Y. Cao, V. Fatemi, S. Fang, K. Watanabe, T. Taniguchi, E. Kaxiras, and P. Jarillo-Herrero, *Nature* **556**, 43 (2018).
- [10] H. S. Arora, R. Polski, Y. Zhang, A. Thomson, Y. Choi, H. Kim, Z. Lin, I. Z. Wilson, X. Xu, J.-H. Chu, *et al.*, *Nature* **583**, 379 (2020).
- [11] A. Kerelsky, L. J. McGilly, D. M. Kennes, L. Xian, M. Yankowitz, S. Chen, K. Watanabe, T. Taniguchi, J. Hone, C. Dean, *et al.*, *Nature* **572**, 95 (2019).
- [12] E. Y. Andrei and A. H. MacDonald, *Nature materials* **19**, 1265 (2020).
- [13] M. Yankowitz, S. Chen, H. Polshyn, Y. Zhang, K. Watanabe, T. Taniguchi, D. Graf, A. F. Young, and C. R. Dean, *Science* **363**, 1059 (2019).
- [14] A. L. Sharpe, E. J. Fox, A. W. Barnard, J. Finney, K. Watanabe, T. Taniguchi, M. A. Kastner, and D. Goldhaber-Gordon, *Science* **365**, 605 (2019).
- [15] X. Lu, P. Stepanov, W. Yang, M. Xie, M. A. Aamir, I. Das, C. Urgell, K. Watanabe, T. Taniguchi, G. Zhang, *et al.*, *Nature* **574**, 653 (2019).
- [16] Y. Saito, J. Ge, K. Watanabe, T. Taniguchi, and A. F. Young, *Nature Physics* **16**, 926 (2020).
- [17] P. Stepanov, I. Das, X. Lu, A. Fahimniya, K. Watanabe, T. Taniguchi, F. H. Koppens, J. Lischner, L. Levitov, and D. K. Efetov, *Nature* **583**, 375 (2020).
- [18] Y. Cao, D. Chowdhury, D. Rodan-Legrain, O. Rubies-Bigorda, K. Watanabe, T. Taniguchi, T. Senthil, and P. Jarillo-Herrero, *Phys. Rev. Lett.* **124**, 076801 (2020).
- [19] H. Polshyn, M. Yankowitz, S. Chen, Y. Zhang, K. Watanabe, T. Taniguchi, C. R. Dean, and A. F. Young, *Nature Physics* **15**, 1011 (2019).
- [20] Y. Xie, B. Lian, B. Jäck, X. Liu, C.-L. Chiu, K. Watanabe, T. Taniguchi, B. A. Bernevig, and A. Yazdani, *Nature* **572**, 101 (2019).
- [21] Y. Jiang, X. Lai, K. Watanabe, T. Taniguchi, K. Haule, J. Mao, and E. Y. Andrei, *Nature* **573**, 91 (2019).
- [22] Y. Choi, J. Kemmer, Y. Peng, A. Thomson, H. Arora, R. Polski, Y. Zhang, H. Ren, J. Alicea, G. Refael, *et al.*, *Nature Physics* **15**, 1174 (2019).
- [23] D. Wong, K. P. Nuckolls, M. Oh, B. Lian, Y. Xie, S. Jeon, K. Watanabe, T. Taniguchi, B. A. Bernevig, and A. Yazdani, *Nature* **582**, 198 (2020).
- [24] X. Liu, Z. Hao, E. Khalaf, J. Y. Lee, Y. Ronen, H. Yoo, D. H. Najafabadi, K. Watanabe, T. Taniguchi, A. Vishwanath, *et al.*, *Nature* **583**, 221 (2020).
- [25] Y. Cao, D. Rodan-Legrain, O. Rubies-Bigorda, J. M. Park, K. Watanabe, T. Taniguchi, and P. Jarillo-Herrero, *Nature* **583**, 215 (2020).
- [26] F. Guinea and N. R. Walet, *Proceedings of the National Academy of Sciences* **115**, 13174 (2018).
- [27] Y.-D. Liao, X.-Y. Xu, Z.-Y. Meng, and J. Kang, *Chinese Physics B* **30**, 017305 (2021).
- [28] Y. Da Liao, Z. Y. Meng, and X. Y. Xu, *Physical Review Letters* **123**, 157601 (2019).
- [29] Yuan Da Liao, Jian Kang, Clara N. Breiø, Xiao Yan Xu, Han-Qing Wu, Brian M. Andersen, Rafael M. Fernandes, and Zi Yang Meng, *Physical Review X* **11**, 011014 (2021).
- [30] X. Y. Xu, K. T. Law, and P. A. Lee, *Physical Review B* **98**, 121406 (2018).
- [31] Y. Saito, Y. Nakamura, M. S. Bahramy, Y. Kohama, J. Ye, Y. Kasahara, Y. Nakagawa, M. Onga, M. Tokunaga, T. Nojima, *et al.*, *Nature Physics* **12**, 144 (2016).
- [32] L. Wang, E.-M. Shih, A. Ghiotto, L. Xian, D. A. Rhodes, C. Tan, M. Claassen, D. M. Kennes, Y. Bai, B. Kim, *et al.*, *Nature materials* **19**, 861 (2020).
- [33] M. Serlin, C. L. Tschirhart, H. Polshyn, Y. Zhang, J. Zhu, K. Watanabe, T. Taniguchi, L. Balents, and A. F. Young, *Science* **367**, 900 (2020).
- [34] C. Shen, Y. Chu, Q. Wu, N. Li, S. Wang, Y. Zhao, J. Tang, J. Liu, J. Tian, K. Watanabe, *et al.*, *Nature Physics* **16**, 520 (2020).
- [35] G. Chen, L. Jiang, S. Wu, B. Lyu, H. Li, B. L. Chittari, K. Watanabe, T. Taniguchi, Z. Shi, J. Jung, *et al.*, *Nature Physics* **15**, 237 (2019).
- [36] G. Chen, A. L. Sharpe, P. Gallagher, I. T. Rosen, E. J. Fox, L. Jiang, B. Lyu, H. Li, K. Watanabe, T. Taniguchi, *et al.*, *Nature* **572**, 215 (2019).
- [37] G. Chen, A. L. Sharpe, E. J. Fox, Y.-H. Zhang, S. Wang, L. Jiang, B. Lyu, H. Li, K. Watanabe, T. Taniguchi, *et al.*, *Nature* **579**, 56 (2020).
- [38] H. Zhou, T. Xie, T. Taniguchi, K. Watanabe, and A. F. Young, *Nature* **598**, 434–438 (2021).
- [39] F. F. Assaad, *Phys. Rev. B* **71**, 075103 (2005).
- [40] Z. Y. Meng, T. C. Lang, S. Wessel, F. F. Assaad, and A. Muramatsu, *Nature* **464**, 847 (2010).
- [41] C.-C. Chang and R. T. Scalettar, *Physical Review Letters* **109**, 026404 (2012).
- [42] Y. Ouyang and X. Y. Xu, *Physical Review B* **104**, L241104 (2021).

- [43] T. C. Lang, Z. Y. Meng, A. Muramatsu, S. Wessel, and F. F. Assaad, *Phys. Rev. Lett.* **111**, 066401 (2013).
- [44] T. Sato, M. Hohenadler, and F. F. Assaad, *Physical Review Letters* **119**, 197203 (2017).
- [45] M. Hohenadler, Z. Y. Meng, T. C. Lang, S. Wessel, A. Muramatsu, and F. F. Assaad, *Phys. Rev. B* **85**, 115132 (2012).
- [46] Z. Y. MENG, H.-H. HUNG, and T. C. LANG, *Modern Physics Letters B* **28**, 1430001 (2014).
- [47] Z. Wang, M. P. Zaletel, R. S. K. Mong, and F. F. Assaad, *Phys. Rev. Lett.* **126**, 045701 (2021).
- [48] Z. Wang, Y. Liu, T. Sato, M. Hohenadler, C. Wang, W. Guo, and F. F. Assaad, *Phys. Rev. Lett.* **126**, 205701 (2021).
- [49] Z. H. Liu, M. Vojta, F. F. Assaad, and L. Janssen, *Physical Review Letters* **128**, 087201 (2022).
- [50] Y. Otsuka, S. Yunoki, and S. Sorella, *Physical Review X* **6**, 011029 (2016).
- [51] F. Parisen Toldin, M. Hohenadler, F. F. Assaad, and I. F. Herbut, *Physical Review B* **91**, 165108 (2015).
- [52] T. C. Lang and A. M. Läuchli, *Physical Review Letters* **123**, 137602 (2019).
- [53] Y. Liu, Z. Wang, T. Sato, M. Hohenadler, C. Wang, W. Guo, and F. F. Assaad, *Nature Communications* **10**, 2658 (2019).
- [54] Z.-X. Li, S.-K. Jian, and H. Yao, arXiv e-prints , arXiv:1904.10975 (2019), arXiv:1904.10975 [cond-mat.str-el].
- [55] Y. Liu, W. Wang, K. Sun, and Z. Y. Meng, *Phys. Rev. B* **101**, 064308 (2020).
- [56] S. Mojtaba Tabatabaei, A.-R. Negari, J. Maciejko, and A. Vaezi, arXiv e-prints , arXiv:2112.09209 (2021), arXiv:2112.09209 [cond-mat.str-el].
- [57] L. Janssen, W. Wang, M. M. Scherer, Z. Y. Meng, and X. Y. Xu, *Phys. Rev. B* **101**, 235118 (2020).
- [58] J. Schwab, L. Janssen, K. Sun, Z. Y. Meng, I. F. Herbut, M. Vojta, and F. F. Assaad, *Phys. Rev. Lett.* **128**, 157203 (2022).
- [59] Y. D. Liao, X. Y. Xu, Z. Y. Meng, and Y. Qi, arXiv:2204.04884 [cond-mat] (2022), arXiv:2204.04884 [cond-mat].
- [60] X. Zhu, Y. Huang, H. Guo, and S. Feng, arXiv e-prints , arXiv:2204.12147 (2022), arXiv:2204.12147 [cond-mat.str-el].
- [61] A. V. Gorshkov, M. Hermele, V. Gurarie, C. Xu, P. S. Julienne, J. Ye, P. Zoller, E. Demler, M. D. Lukin, and A. M. Rey, *Nature Physics* **6**, 289 (2010).
- [62] M. A. Cazalilla and A. M. Rey, *Reports on Progress in Physics* **77**, 124401 (2014).
- [63] X. Zhang, G. Pan, Y. Zhang, J. Kang, and Z. Y. Meng, *Chinese Physics Letters* **38**, 077305 (2021).
- [64] G. Pan, X. Zhang, H. Li, K. Sun, and Z. Y. Meng, *Phys. Rev. B* **105**, L121110 (2022).
- [65] X. Zhang, K. Sun, H. Li, G. Pan, and Z. Y. Meng, arXiv e-prints , arXiv:2111.10018 (2021), arXiv:2111.10018 [cond-mat.supr-con].
- [66] Y. Ran, M. Hermele, P. A. Lee, and X.-G. Wen, *Phys. Rev. Lett.* **98**, 117205 (2007).
- [67] X. Y. Xu, Y. Qi, L. Zhang, F. F. Assaad, C. Xu, and Z. Y. Meng, *Phys. Rev. X* **9**, 021022 (2019).
- [68] N. Ma, G.-Y. Sun, Y.-Z. You, C. Xu, A. Vishwanath, A. W. Sandvik, and Z. Y. Meng, *Phys. Rev. B* **98**, 174421 (2018).
- [69] N. Ma, Y.-Z. You, and Z. Y. Meng, *Phys. Rev. Lett.* **122**, 175701 (2019).
- [70] Y.-Y. He, H.-Q. Wu, Y.-Z. You, C. Xu, Z. Y. Meng, and Z.-Y. Lu, *Phys. Rev. B* **94**, 241111 (2016).
- [71] W. Wang, D.-C. Lu, X. Y. Xu, Y.-Z. You, and Z. Y. Meng, *Phys. Rev. B* **100**, 085123 (2019).
- [72] N. F. Mott, *Proceedings of the Physical Society. Section A* **62**, 416 (1949).
- [73] S. Sorella and E. Tosatti, *Europhysics Letters (EPL)* **19**, 699 (1992).
- [74] C. Wu and S.-C. Zhang, *Physical Review B* **71**, 155115 (2005).
- [75] G. Pan and Z. Y. Meng, arXiv e-prints , arXiv:2204.08777 (2022), arXiv:2204.08777 [cond-mat.str-el].
- [76] F. Assaad and H. Evertz, in *Computational Many-Particle Physics*, Vol. 739, edited by H. Fehske, R. Schneider, and A. Weiße (Springer Berlin Heidelberg, Berlin, Heidelberg, 2008) pp. 277–356.
- [77] The implementation of three different quantum Monte Carlo simulation algorithms, more data of structure factors as a function of interaction strength and single-particle gap near QCP, and the dynamical spin spectrum of free π -flux model, are presented in this Supplemental Material.
- [78] P. A. Lee, N. Nagaosa, and X.-G. Wen, *Rev. Mod. Phys.* **78**, 17 (2006).
- [79] S.-S. Lee and P. A. Lee, *Phys. Rev. Lett.* **95**, 036403 (2005).
- [80] M. Hermele, T. Senthil, and M. P. A. Fisher, *Phys. Rev. B* **72**, 104404 (2005).
- [81] D. H. Kim, P. A. Lee, and X.-G. Wen, *Phys. Rev. Lett.* **79**, 2109 (1997).
- [82] M. Hermele, T. Senthil, and M. P. A. Fisher, *Phys. Rev. B* **76**, 149906 (2007).
- [83] X.-G. Wen and P. A. Lee, *Phys. Rev. Lett.* **76**, 503 (1996).
- [84] É. Dupuis, R. Boyack, and W. Witczak-Krempa, arXiv e-prints , arXiv:2108.05922 (2021), arXiv:2108.05922 [cond-mat.str-el].
- [85] V. Calvera and C. Wang, arXiv:2103.13405 [cond-mat, physics:hep-lat, physics:hep-th] (2021).
- [86] T. Senthil, L. Balents, S. Sachdev, A. Vishwanath, and M. P. A. Fisher, *Physical Review B* **70**, 144407 (2004).
- [87] Y. Q. Qin, Y.-Y. He, Y.-Z. You, Z.-Y. Lu, A. Sen, A. W. Sandvik, C. Xu, and Z. Y. Meng, *Phys. Rev. X* **7**, 031052 (2017).
- [88] H. R. Fiebig and R. M. Woloshyn, *Phys. Rev. D* **42**, 3520 (1990).
- [89] I. F. Herbut and B. H. Seradjeh, *Phys. Rev. Lett.* **91**, 171601 (2003).
- [90] F. S. Nogueira and H. Kleinert, *Phys. Rev. B* **77**, 045107 (2008).
- [91] N. Karthik and R. Narayanan, *Phys. Rev. D* **100**, 054514 (2019).
- [92] N. Karthik and R. Narayanan, *Phys. Rev. Lett.* **125**, 261601 (2020).
- [93] S. Albayrak, R. S. Erramilli, Z. Li, D. Poland, and Y. Xin, *Phys. Rev. D* **105**, 085008 (2022).
- [94] S. Pujari, T. C. Lang, G. Murthy, and R. K. Kaul, *Phys. Rev. Lett.* **117**, 086404 (2016).
- [95] M. M. Scherer and I. F. Herbut, *Physical Review B* **94**, 205136 (2016).
- [96] Z.-X. Li, Y.-F. Jiang, S.-K. Jian, and H. Yao, *Nature Communications* **8**, 314 (2017).
- [97] L. Classen, I. F. Herbut, and M. M. Scherer, *Physical Review B* **96**, 115132 (2017).
- [98] E. Torres, L. Classen, I. F. Herbut, and M. M. Scherer, *Physical Review B* **97**, 125137 (2018).
- [99] Z. Zhou, C. Wu, and Y. Wang, *Physical Review B* **97**, 195122 (2018).
- [100] B. Rosenstein, Hoi-Lai Yu, and A. Kovner, *Physics Letters B* **314**, 381 (1993).
- [101] N. Zerf, L. N. Mihaila, P. Marquard, I. F. Herbut, and M. M. Scherer, *Physical Review D* **96**, 096010 (2017).
- [102] A. Nahum, J. T. Chalker, P. Serna, M. Ortúñoz, and A. M. Somoza, *Phys. Rev. X* **5**, 041048 (2015).
- [103] A. Nahum, P. Serna, J. Chalker, M. Ortúñoz, and A. Somoza, *Physical Review Letters* **115**, 267203 (2015).

- [104] F. F. Assaad and T. Grover, *Phys. Rev. X* **6**, 041049 (2016).
- [105] S. Gazit, M. Randeria, and A. Vishwanath, *Nature Physics* **13**, 484 (2017).
- [106] A. W. Sandvik, *Phys. Rev. B* **57**, 10287 (1998).
- [107] K. S. D. Beach, arXiv e-prints , cond-mat/0403055 (2004), [arXiv:cond-mat/0403055 \[cond-mat.str-el\]](#).
- [108] O. F. Syljuåsen, *Phys. Rev. B* **78**, 174429 (2008).
- [109] H. Shao, Y. Q. Qin, S. Capponi, S. Chesi, Z. Y. Meng, and A. W. Sandvik, *Phys. Rev. X* **7**, 041072 (2017).
- [110] A. W. Sandvik, *Phys. Rev. E* **94**, 063308 (2016).
- [111] G.-Y. Sun, Y.-C. Wang, C. Fang, Y. Qi, M. Cheng, and Z. Y. Meng, *Phys. Rev. Lett.* **121**, 077201 (2018).
- [112] Y.-C. Wang, Z. Yan, C. Wang, Y. Qi, and Z. Y. Meng, *Phys. Rev. B* **103**, 014408 (2021).
- [113] Y.-C. Wang, M. Cheng, W. Witczak-Krempa, and Z. Y. Meng, *Nature Communications* **12**, 5347 (2021).
- [114] Z. Yan, Y.-C. Wang, N. Ma, Y. Qi, and Z. Y. Meng, *npj Quantum Mater.* , 39 (2021).
- [115] C. Zhou, Z. Yan, H.-Q. Wu, K. Sun, O. A. Starykh, and Z. Y. Meng, *Phys. Rev. Lett.* **126**, 227201 (2021).
- [116] W. Jiang, Y. Liu, A. Klein, Y. Wang, K. Sun, A. V. Chubukov, and Z. Y. Meng, arXiv e-prints , arXiv:2105.03639 (2021), [arXiv:2105.03639 \[cond-mat.str-el\]](#).
- [117] Z. Yan, R. Samajdar, Y.-C. Wang, S. Sachdev, and Z. Y. Meng, arXiv e-prints , arXiv:2202.11100 (2022), [arXiv:2202.11100 \[cond-mat.str-el\]](#).
- [118] H. Shao and A. W. Sandvik, arXiv e-prints , arXiv:2202.09870 (2022), [arXiv:2202.09870 \[cond-mat.str-el\]](#).
- [119] C. Zhou, M.-Y. Li, Z. Yan, P. Ye, and Z. Y. Meng, arXiv e-prints , arXiv:2203.13274 (2022), [arXiv:2203.13274 \[cond-mat.str-el\]](#).
- [120] H. Li, Y. D. Liao, B.-B. Chen, X.-T. Zeng, X.-L. Sheng, Y. Qi, Z. Y. Meng, and W. Li, *Nat. Commun.* **11**, 1111 (2020).
- [121] Z. Hu, Z. Ma, Y.-D. Liao, H. Li, C. Ma, Y. Cui, Y. Shangguan, Z. Huang, Y. Qi, W. Li, Z. Y. Meng, J. Wen, and W. Yu, *Nature Communications* **11**, 5631 (2020).
- [122] T. Senthil, A. Vishwanath, L. Balents, S. Sachdev, and M. P. A. Fisher, *Science* **303**, 1490 (2004).
- [123] B. Dalla Piazza, M. Mourigal, N. B. Christensen, G. J. Nilsen, P. Tregenna-Piggott, T. G. Perring, M. Enderle, D. F. McMorrow, D. A. Ivanov, and H. M. Rönnnow, *Nature Physics* **11**, 62 (2015).
- [124] J. Guo, G. Sun, B. Zhao, L. Wang, W. Hong, V. A. Sidorov, N. Ma, Q. Wu, S. Li, Z. Y. Meng, A. W. Sandvik, and L. Sun, *Phys. Rev. Lett.* **124**, 206602 (2020).
- [125] G. Sun, N. Ma, B. Zhao, A. W. Sandvik, and Z. Y. Meng, *Chinese Physics B* **30**, 067505 (2021).
- [126] Y. Cui, L. Liu, H. Lin, K.-H. Wu, W. Hong, X. Liu, C. Li, Z. Hu, N. Xi, S. Li, R. Yu, A. W. Sandvik, and W. Yu, arXiv e-prints , arXiv:2204.08133 (2022), [arXiv:2204.08133 \[cond-mat.str-el\]](#).
- [127] L. Ding, P. Manuel, S. Bachus, F. Grußler, P. Gegenwart, J. Singleton, R. D. Johnson, H. C. Walker, D. T. Adroja, A. D. Hillier, and A. A. Tsirlin, *Phys. Rev. B* **100**, 144432 (2019).
- [128] S. Kundu, A. Shahee, A. Chakraborty, K. M. Ranjith, B. Koo, J. Sichelschmidt, M. T. F. Telling, P. K. Biswas, M. Baenitz, I. Dasgupta, S. Pujari, and A. V. Mahajan, *Phys. Rev. Lett.* **125**, 267202 (2020).
- [129] Z. Zeng, X. Ma, S. Wu, H.-F. Li, Z. Tao, X. Lu, X.-h. Chen, J.-X. Mi, S.-J. Song, G.-H. Cao, G. Che, K. Li, G. Li, H. Luo, Z. Y. Meng, and S. Li, *Phys. Rev. B* **105**, L121109 (2022).
- [130] J. B. Marston, *Phys. Rev. Lett.* **64**, 1166 (1990).
- [131] O. I. Motrunich, *Phys. Rev. B* **72**, 045105 (2005).
- [132] A. W. Sandvik, *Physical Review Letters* **98**, 227202 (2007).

Supplemental Material for "Gross-Neveu criticality and Dirac quantum spin liquid emerging in $SU(4)$ extended Hubbard model on square lattice"

I. QMC METHODS

A. Finite temperature auxiliary field QMC method

As mentioned in the main text, we investigate an half-filling π -flux extended Hubbard model on square lattice, its Hamiltonian is $H = H_0 + H_U$ with non-interacting part $H_0 = -\sum_{\langle ij \rangle, \alpha} t_{ij} (c_{i\alpha}^\dagger c_{j\alpha} + \text{H.c.})$ and interacting part $H_U = U \sum_{\square} (n_{\square} - 2)^2$. Since H_0 and H_U do not commute, we use Trotter decomposition to separate H_0 and H_U in the imaginary time propagation

$$Z = \text{Tr} \left[e^{-\beta(H-\mu N)} \right] = \text{Tr} \left[\left(e^{-\Delta\tau H_U} e^{-\Delta\tau H_t} \right)^M \right] + \mathcal{O}(\Delta\tau^2), \quad (\text{S1})$$

where Z is the partition function, $\beta = M\Delta\tau$ is the inverse temperature, μ is chemical potential and equals 0 at half-filling. In QMC method, we can only deal with quadratic fermionic operator, while H_U contains the quartic term, thus we should employ a Hubbard-Stratonovich (HS) decomposition as

$$e^{-\Delta\tau U(n_{\square}-2)^2} = \frac{1}{4} \sum_{\{s_{\square,\tau}\}} \gamma(s_{\square,\tau}) e^{-2\alpha\eta(s_{\square,\tau})} e^{\alpha\eta(s_{\square,\tau})n_{\square}} \quad (\text{S2})$$

with $\alpha = \sqrt{-\Delta\tau U}$, $\gamma(\pm 1) = 1 + \sqrt{6}/3$, $\gamma(\pm 2) = 1 - \sqrt{6}/3$, $\eta(\pm 1) = \pm\sqrt{2(3 - \sqrt{6})}$, $\eta(\pm 2) = \pm\sqrt{2(3 + \sqrt{6})}$ and the sum symbol is taken over the auxiliary fields $s_{\square,\tau}$ on each τ -th time slice square plaquette. Now, the interacting part is transformed into quadratic term but coupled with an auxiliary field. Following simulations are based on the single-particle basis $c = \{c_1, c_2 \dots c_N\}$, $N = L \times L$ is the system size, so we can use the matrix notation K and V to represent H_0 and H_U operators. We define the imaginary time propagators

$$\begin{aligned} U_{s_{\square}}(\tau_2, \tau_1) &= \prod_{m=m_1+1}^{m_2} e^{c^\dagger V(s_{\square, m\Delta\tau}) c} e^{-\Delta\tau c^\dagger K c}, \\ B_{s_{\square}}(\tau_2, \tau_1) &= \prod_{m=m_1+1}^{m_2} e^{V(s_{\square, m\Delta\tau})} e^{-\Delta\tau K}, \end{aligned} \quad (\text{S3})$$

where $m_1\Delta\tau = \tau_1$ and $m_2\Delta\tau = \tau_2$. Then partition function Z can be rewritten as

$$Z = \sum_{\{s_{\square,\tau}\}} \text{Tr} [U_{s_{\square}}(\beta, 0)] \prod_{m=1}^M \gamma(s_{\square, m\Delta\tau}) e^{-2\alpha\eta(s_{\square, m\Delta\tau})} = \sum_{\{s_{\square,\tau}\}} \det [1 + B_{s_{\square}}(\beta, 0)] \prod_{m=1}^M \gamma(s_{\square, m\Delta\tau}) e^{-2\alpha\eta(s_{\square, m\Delta\tau})}. \quad (\text{S4})$$

Physical observables are measured according to $\langle O \rangle = \frac{\text{Tr}[e^{-\beta H} O]}{\text{Tr}[e^{-\beta H}]}$. The equal-time single-particle Green function is given by $G_{i,j}(\tau, \tau) = \langle c_{i,\tau} c_{j,\tau}^\dagger \rangle = (1 + B_{s_{\square}}(\tau, 0) B_{s_{\square}}(\beta, \tau))_{i,j}^{-1}$, and the dynamical single-particle Green function is given by $G_{i,j}(\tau_1, \tau_2) = \langle c_{i,\tau_1} c_{j,\tau_2}^\dagger \rangle = -[(\mathbf{1} - \mathbf{G}(\tau_1, \tau_1)) B_{s_{\square}}^{-1}(\tau_2, \tau_1)]_{i,j}$. Other physical observables can be calculated from single-particle Green function through Wick's theorem. More technical details of the finite-temperature QMC algorithms can be found in the reference book [76].

B. Projection QMC method

Since we also want to investigate the ground state properties, the projection quantum Monte Carlo (PQMC) method is a good choice. We can calculate the ground state wave function $|\Psi_0\rangle$ through the projection of a trial wave function $|\Psi_T\rangle$ as $|\Psi_0\rangle = \lim_{\Theta \rightarrow \infty} e^{-\frac{\Theta}{2}\mathbf{H}} |\Psi_T\rangle$, where Θ is the projection length. Actually, in PQMC method, we use $\langle \Psi_T | e^{-\Theta H} |\Psi_T \rangle$ to replace the role of partition function in finite-temperature version. Physical observables O can be measured according to

$$\langle O \rangle = \frac{\langle \Psi_0 | O | \Psi_0 \rangle}{\langle \Psi_0 | \Psi_0 \rangle} = \lim_{\Theta \rightarrow \infty} \frac{\langle \Psi_T | e^{-\frac{\Theta}{2}\mathbf{H}} O e^{-\frac{\Theta}{2}\mathbf{H}} | \Psi_T \rangle}{\langle \Psi_T | e^{-\Theta \mathbf{H}} | \Psi_T \rangle}. \quad (\text{S5})$$

After the Trotter and HS decomposition, we have

$$\langle \Psi_T | e^{-\Theta H} | \Psi_T \rangle = \sum_{\{s_{\square, \tau}\}} \left[\left(\prod_{\tau} \prod_{\square} \gamma(s_{\square, \tau}) e^{-2\alpha \eta(s_{\square, \tau})} \right) \det [P^\dagger B(\Theta, 0) P] \right] \quad (\text{S6})$$

here P is the coefficient matrix of trial wave function $|\Psi_T\rangle$; B matrix is defined as $B(\tau + 1, \tau) = e^{V_\tau} e^{-\Delta_\tau K}$ and has a property $B(\tau_3, \tau_1) = B(\tau_3, \tau_2)B(\tau_2, \tau_1)$. In the practice, we choose the ground state wavefunction of the half-filled non-interacting parts of Hamiltonian as the trial wave function. The Monte Carlo sampling of auxiliary fields are further performed based on the weight defined in the sum of Eq. (S6). Single particle observables are measured by Green's function directly and many body correlation functions are measured from the products of single-particle Green's function based on their corresponding form after Wick-decomposition. The equal time Green's function are calculated as

$$G(\tau, \tau) = 1 - R(\tau) (L(\tau)R(\tau))^{-1} L(\tau) \quad (\text{S7})$$

with $R(\tau) = B(\tau, 0)P$, $L(\tau) = P^\dagger B(\Theta, \tau)$. The imaginary-time displaced Green's function $G(\tau, 0) \equiv \langle c\left(\frac{\tau}{2}\right) c^\dagger\left(-\frac{\tau}{2}\right) \rangle$ are calculated as

$$\langle c\left(\frac{\tau}{2}\right) c^\dagger\left(-\frac{\tau}{2}\right) \rangle = \frac{\langle \Psi_T | e^{-\left(\frac{\Theta}{2} + \frac{\tau}{2}\right)H} c e^{-\tau H} c^\dagger e^{-\left(\frac{\Theta}{2} - \frac{\tau}{2}\right)H} | \Psi_T \rangle}{\langle \Psi_T | e^{-\Theta H} | \Psi_T \rangle} \quad (\text{S8})$$

More technique details of PQMC method, please also refer to Refs [76].

C. Infinite U QMC algorithm

For infinite U calculation, we use following formula to perform the $SU(N)$ infinite U projection [42]

$$e^{-\Delta_\tau U(n_{\square}-2)^2} \Big|_{U \rightarrow +\infty} = \frac{1}{M} \sum_{s_{\square, \tau}=1}^M e^{\frac{i8\pi s_{\square, \tau}}{M}(n_{\square} - \frac{N}{2})}, \quad (\text{S9})$$

where we can set $M = 2N + 1$. As the infinite U term has now been replaced by fermion bilinears coupled to auxiliary fields, we can further use above finite temperature and projection QMC scheme to perform the calculation.

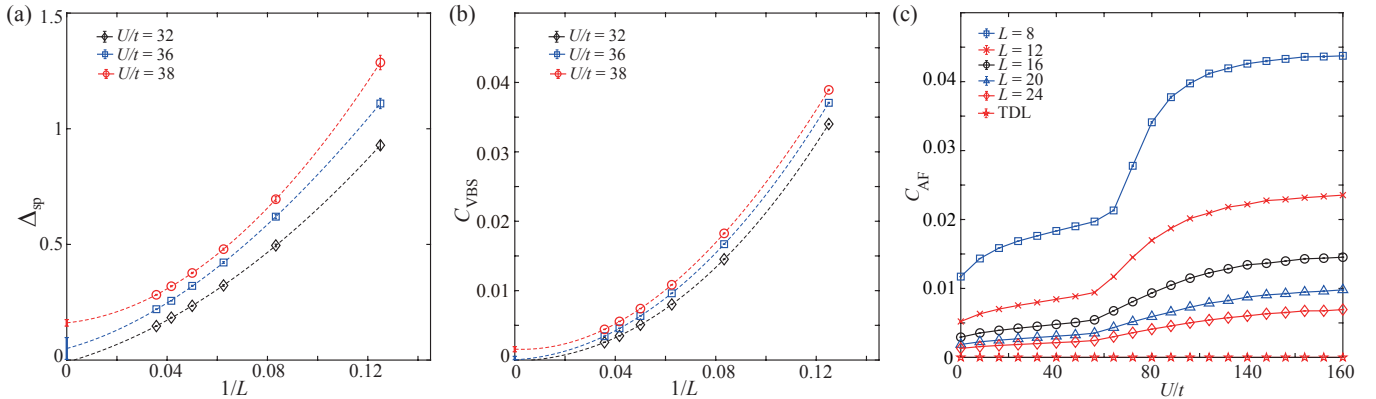


FIG. S1. (a) $1/L$ extrapolation of single-particle gap. (b) $1/L$ extrapolation of VBS structure factor. The dash lines are obtained by cubic polynomial fitting with least squares method. (c) The AF structure factors as function of interaction strength. Error bars are smaller than the symbols.

II. OTHER QMC DATA

A. The single-particle gap and VBS order parameter near QCP of SM-VBS

The Dirac SM to VBS phase transition is a transition from massless Dirac fermion to insulator, thus single-particle gap Δ_{sp} will open at Dirac cones, i.e. at the momentum point \mathbf{K}_0 . We can extract $\Delta_{sp}(\mathbf{K}_0, L)$ from a fit to the asymptotic long imaginary

time behavior of the single-particle Green's function $G(\mathbf{k}, \tau, L) = (1/L^4) \sum_{i,j,\sigma} e^{i\mathbf{k}\cdot(\mathbf{r}_i-\mathbf{r}_j)} \langle c_{i,\sigma}^\dagger(\tau) c_{j,\sigma}(0) \rangle \propto e^{-\Delta_{\text{sp}}(\mathbf{k}, L)\tau}$, then extrapolate it to the thermodynamic limit (TDL). As shown in Fig. S1 (a), it is clear that $\Delta_{\text{sp}}(\mathbf{K}_0, L \rightarrow \infty) \rightarrow 0$ at $U/t = 32$ in the SM phase, $\Delta_{\text{sp}}(\mathbf{K}_0, L \rightarrow \infty) > 0$ at $U/t = 38$ in the VBS phase, and $\Delta_{\text{sp}}(\mathbf{K}_0, L \rightarrow \infty) \sim 0$ at $U_c/t = 36$. The $1/L$ extrapolation of C_{VBS} has the similar behavior as $\Delta_{\text{sp}}(\mathbf{K}_0, L)$ near U_c , as shown in Fig. S1 (b).

B. The absence of AF order

In Hubbard-like model, the AF order usually dominate when VBS order become weak in strong coupling region [30, 59]. Here, we demonstrate that the AF order is absent in our model. We define the structure factor of AF order as $C_{\text{AF}}(\mathbf{k}, L) \equiv \frac{1}{L^4} \sum_{\mathbf{r}} e^{-i\mathbf{q}\cdot\mathbf{r}} \sum_{\alpha,\beta} \langle S_\beta^\alpha(i) S_\alpha^\beta(j) \rangle$, C_{AF} will peak at momentum point \mathbf{M} for AF order. We can perform $1/L$ extrapolation of $C_{\text{AF}}(\mathbf{M}, L)$ to get the AF structure factor at TDL, marked as $C_{\text{AF}}(\mathbf{M}, \infty)$. As shown in Fig. S1 (c), $C_{\text{AF}}(\mathbf{M}, \infty)$ vanish at whole interaction strength range $U/t \in [0, 160]$, which mean the AF order is absent in our model.

III. DYNAMICAL SPIN SPECTRUM OF FREE π -FLUX MODEL

We have a free $SU(4)$ π -flux model on square lattice with Hamiltonian

$$H = - \sum_{\langle ij \rangle, \alpha} t_{ij} \left(c_{ia}^\dagger c_{ja} + \text{H.c.} \right). \quad (\text{S10})$$

, and consider two-site unit cell, with inner cell coordinates $\mathbf{v}_1 = (0, 0)$, $\mathbf{v}_2 = (1, 0)$. We transform the Hamiltonian to the momentum space,

$$H = -t \sum_{\mathbf{k}} c_{\mathbf{k}}^\dagger \begin{pmatrix} 2 \cos k_y & 1 + e^{-2ik_x} \\ 1 + e^{2ik_x} & -2 \cos k_y \end{pmatrix} c_{\mathbf{k}} \quad (\text{S11})$$

where $c_{\mathbf{k}} = (c_{1,\mathbf{k}}, c_{2,\mathbf{k}})^T$. We further write H in the diagonal basis

$$\begin{aligned} H &= \sum_{\mathbf{k}, a, b, m, n} c_{a,\mathbf{k}}^\dagger (U_{\mathbf{k}})_{am} (D_{\mathbf{k}})_{mn} (U_{\mathbf{k}}^{-1})_{nb} c_{b,\mathbf{k}} \\ &\equiv \sum_{\mathbf{k}, a} \epsilon_{a,\mathbf{k}} f_{a,\mathbf{k}}^\dagger f_{a,\mathbf{k}} \end{aligned} \quad (\text{S12})$$

where we use $a, b, m, n \in [1, 2]$ to denote sublattice index, $(D_{\mathbf{k}})_{mn} = \delta_{mn} \epsilon_{m,\mathbf{k}}$, $\epsilon_{m,\mathbf{k}} = \pm 2 \sqrt{\cos^2 k_x + \cos^2 k_y}$ is the dispersion, and we define $f_{a,\mathbf{k}} \equiv U_{\mathbf{k}}^{-1} c_{a,\mathbf{k}}$. Here the dispersion is flavor degenerate, and we have omitted the flavor index, . The sum is over \mathbf{k} in the small (rectangle) BZ, i.e. $k_x \in (-\frac{\pi}{2}, \frac{\pi}{2})$ and $k_y \in (-\pi, \pi)$.

To calculate spin spectrum, we can use fluctuation-dissipation theorem, which relates the spin spectrum to the spin susceptibility. The spin susceptibility has following form

$$\chi_{ab}^R(\mathbf{r} - \mathbf{r}', t - t') = -i\theta(t - t') \sum_{\mu\nu} \langle [S_\nu^\mu(\mathbf{r}, a, t), S_\mu^\nu(\mathbf{r}', b, t')] \rangle. \quad (\text{S13})$$

Fourier transform to momentum space, we get

$$\chi_{ab}^R(\mathbf{q}, t - t') = -i\theta(t - t') \frac{1}{V} \sum_{\mu\nu} \langle [S_\nu^\mu(\mathbf{q}, a, t), S_\mu^\nu(-\mathbf{q}, b, t')] \rangle \quad (\text{S14})$$

, where $S_\beta^\alpha(\mathbf{k}, a, t) = c_{\mathbf{k},\alpha}^\dagger c_{\mathbf{k},\beta} - \frac{\delta_{\alpha,\beta}}{4} \sum_{\gamma} c_{\mathbf{k},\gamma}^\dagger c_{\mathbf{k},\gamma}$ are the $SU(4)$ spin full operators with $\alpha, \beta, \gamma \in [1, 4]$.

For non-interacting $SU(4)$ case, the time dependence of spin operator is given by

$$\begin{aligned} S_\nu^\mu(\mathbf{q}, a, t) &= \sum_{\mathbf{k}} e^{iHt} (c_{a,\mathbf{k},\mu}^\dagger c_{a,\mathbf{k}+\mathbf{q},\nu} - \frac{\delta_{\mu\nu}}{N} \sum_{\lambda} c_{a,\mathbf{k},\lambda}^\dagger c_{a,\mathbf{k}+\mathbf{q},\lambda}) e^{-iHt} \\ &= \sum_{\mathbf{k}} \sum_{mn} (U_{\mathbf{k}}^{-1})_{ma} (U_{\mathbf{k}+\mathbf{q}})_{an} (f_{m,\mathbf{k},\mu}^\dagger f_{n,\mathbf{k}+\mathbf{q},\nu} - \frac{\delta_{\mu\nu}}{N} \sum_{\rho} f_{m,\mathbf{k},\rho}^\dagger f_{n,\mathbf{k}+\mathbf{q},\rho}) e^{i(\epsilon_{m,\mathbf{k}} - \epsilon_{n,\mathbf{k}+\mathbf{q}})t} \end{aligned} \quad (\text{S15})$$

Therefore

$$\chi_{ab}^R(\mathbf{q}, t - t') = -i\theta(t - t') \frac{N^2 - 1}{V} \sum_{\mathbf{k}} \sum_{mn} (U_{\mathbf{k}}^{-1})_{ma} (U_{\mathbf{k}+\mathbf{q}})_{an} (U_{\mathbf{k}+\mathbf{q}}^{-1})_{nb} (U_{\mathbf{k}})_{bm} [n_F(\epsilon_{m,\mathbf{k}}) - n_F(\epsilon_{n,\mathbf{k}+\mathbf{q}})] e^{i(\epsilon_{m,\mathbf{k}} - \epsilon_{n,\mathbf{k}+\mathbf{q}})(t - t')} \quad (\text{S16})$$

Perform Fourier transformation to frequency space, we get

$$\chi_{ab}^R(\mathbf{q}, \omega) = \frac{N^2 - 1}{V} \sum_{\mathbf{k}} \sum_{mn} (U_{\mathbf{k}}^{-1})_{ma} (U_{\mathbf{k}+\mathbf{q}})_{an} (U_{\mathbf{k}+\mathbf{q}}^{-1})_{nb} (U_{\mathbf{k}})_{bm} \frac{n_F(\epsilon_{m,\mathbf{k}}) - n_F(\epsilon_{n,\mathbf{k}+\mathbf{q}})}{\epsilon_{m,\mathbf{k}} - \epsilon_{n,\mathbf{k}+\mathbf{q}} + \omega + i\eta} \quad (\text{S17})$$

To get the full spin spectrum, we should keep in mind that above derivation is in small BZ. Now we consider the spin correlation on a square lattice (one site unit cell), and relate it to above formula.

$$\chi^R(\mathbf{r}_i - \mathbf{r}_j, t - t') = -i\theta(t - t') \sum_{\mu\nu} \langle [S_{\nu}^{\mu}(\mathbf{r}_i, t), S_{\mu}^{\nu}(\mathbf{r}_j, t')] \rangle \quad (\text{S18})$$

denote $\mathbf{r}_i = \mathbf{r} + \mathbf{v}_a$, $\mathbf{r}_j = \mathbf{r}' + \mathbf{v}_b$, we have

$$\chi^R(\mathbf{r} + \mathbf{v}_a - \mathbf{r}' - \mathbf{v}_b, t - t') = -i\theta(t - t') \sum_{\mu\nu} \langle [S_{\nu}^{\mu}(\mathbf{r}, a, t), S_{\mu}^{\nu}(\mathbf{r}', b, t')] \rangle \equiv \chi_{ab}^R(\mathbf{r} - \mathbf{r}', t - t') \quad (\text{S19})$$

Perform fourier transformation, we get following relation

$$\chi^R(\mathbf{q}, \omega) = \sum_{ab} \chi_{ab}^R(\mathbf{q}, \omega) e^{-i\mathbf{q}(\mathbf{v}_a - \mathbf{v}_b)}, \quad (\text{S20})$$

and the full spin spectrum is

$$S(\mathbf{q}, \omega) = -2\text{Im}\chi^R(\mathbf{q}, \omega) \quad (\text{S21})$$